Ages and metallicities of eight star clusters and their surrounding fields in the inner disc of the Large Magellanic Cloud

Doug Geisler,[1]★ Andrés E. Piatti,[2]★ Eduardo Bica[3]★ and Juan J. Clariá[4]★

[1]*Grupo de Astronomía, Departamento de Física, Universidad de Concepción, Casilla 160-C, Concepción, Chile*
[2]*Instituto de Astronomía y Fisica del Espacio, CC 67, Suc. 28, 1428, Capital Federal, Argentina*
[3]*Universidade Federal do Rio Grande do Sul, Depto. de Astronomía, CP 15051, Porto Alegre, 91500-970, Brazil*
[4]*Observatorio Astronómico, Laprida 854, 5000 Córdoba, Argentina*

ABSTRACT

We present Washington system colour–magnitude diagrams for 8 star clusters and their surrounding fields which, with one exception, lie within the inner parts of the Large Magellanic Cloud (LMC) disc. Careful attention is paid to separating out the cluster and field star distributions. Ages and metallicities are then determined in a consistent manner for both populations in two different ways. We first compare the colour–magnitude diagrams (CMDs) with new theoretical isochrones in the Washington system. We also derive ages using the magnitude difference between the red clump and the turnoff, and derive metallicities by comparing the giant branches to standard calibrating clusters. For this latter metallicity derivation, we present age-dependent metallicity corrections for intermediate age clusters (IACs) based on the new isochrones. The two methods for both age and metallicity determination are in good agreement with each other. All clusters are found to be IACs (1–3 Gyr), with [Fe/H] from −0.4 to −0.9. We find that the stellar population of each star cluster is generally quite similar to that of the field where it is embedded, sharing its mean age and metallicity. Combining the present sample with a revision of that of Bica et al. studied similarly, we find that our metallicities for IACs are intermediate in metallicity to those for clusters of similar age studied by Olszewski et al. and by Beasley, Hoyle & Sharples. A combined age–metallicity relation is presented which shows that LMC clusters formed between 1–3 Gyr ago with a mean metallicity (–0.5 dex) and metallicity spread (0.23 dex) independent of age. Good agreement is found with the bursting model of Pagel & Tautvaiˇvienė. No evidence for a metallicity gradient is found.

Key words: techniques: photometric – Magellanic Clouds – galaxies: star clusters.

1 INTRODUCTION

A simple view of the Large Magellanic Cloud (LMC) through a small telescope is enough to convince even the novice that this galaxy is a star cluster factory. The estimated number of clusters in the LMC is ∼4200 (Hodge 1988). Since the pioneering work of Hodge (1960), Gascoigne (1966) and Hesser, Ugarte & Hartwick (1976), it has been known that at least the brightest LMC clusters, although rivalling those in our Galaxy in terms of numbers of stars, include a much wider range of integrated colours and colour–magnitude diagram (CMD) properties. These and many subsequent studies have shown that the LMC possesses both a small number of Galactic globular-cluster-like objects, being both massive and old (>10 Gyr), as well as a very large number of clusters that are popu-

lous but much younger (≲3 Gyr), with virtually no Galactic counterparts. Both the Galaxy and the LMC, then, started their lives making a substantial number of massive clusters but soon lost this ability and the Galaxy never recovered it, while the LMC managed to restart its cluster-making machinery a few Gyr ago and make it work better than ever. Meanwhile, the SMC, although a bit slow to get started, has managed to generate massive clusters continuously during its lifetime. Remarkably, the resulting age – metallicity relations of the two Clouds are very similar, despite their diverse cluster formation histories (Piatti et al. 2002). These fascinating galactic similarities and differences have inspired a generation of astronomers to attempt to understand the underlying reasons for their existence.

In particular, the nature and cause of the huge cluster age gap in the LMC remains of great interest. Several searches for clusters that might help fill in this gap have proved unsuccessful (Da Costa 1991, Geisler et al. 1997 – herafter G97; Rich, Shara & Zurek 2001). During more than half of its life, this 'star cluster factory' only succeeded

★E-mail: doug@kukita.cfm.udec.cl (DG); andres@iafe.uba.ar (AEP); bica@if.ufrgs.br (EB); claria@mail.oac.uncor.edu (JJC)

in making a single star cluster. A variety of *HST* observations, meanwhile, have made it increasingly clear that a corresponding age gap in the field stars does **not** exist (Holtzman et al. 1999; Olsen 1999; Smecker-Hane et al. 2002). The cluster age gap prevents us from using them to tell us details about the chemical evolution and star formation history of the LMC during this long period. However, the pronounced advantages of deriving accurate ages and metallicities for clusters as opposed to single stars (e.g. Olszewski et al. 1991; Bica et al. 1998 – hereafter B98) do allow them to play a leading role in investigating chemical evolution and cluster formation history during those epochs when the factory was in business. In particular, tracing the details of the recent burst(s) in cluster and star formation that occurred over the last few Gyr requires the measurement of ages and metallicities for a large number of clusters. This is the main motivation of the present study. The work of Smecker-Hane et al. (2002) has made it clear that the various components of the LMC, e.g. the bar and an inner disc field, have experienced quite different star formation and likely chemical evolution histories, and further detailed knowledge of the various components is required to piece together their pasts. We note that this is one in a series of papers devoted to the study of LMC clusters that we have carried out over the past few years, including G97, B98, Santos et al. (1999), Piatti et al. (1999) and Piatti et al. (2002). This work is complementary to such studies as those of Cole, Smecker-Hane & Gallagher (2000) or Hill et al. (2000) who are using other techniques, e.g. Ca triplet spectroscopy, Strömgren photometry or high-resolution abundance analysis, to probe the temporal and chemical evolution of the LMC.

The data analysed here were originally taken as part of the G97 search for age-gap clusters. In that paper, ages were derived for all but one of the present sample of clusters. However, we have decided to revisit these clusters for the following reasons.

(1) In G97, we performed a crude age analysis on a much larger number of clusters in order to determine simply whether a cluster fell within the age gap or not. Here we undertake a more detailed investigation of each cluster, in particular with more careful attention to the optimum separation of the cluster from its surrounding field, in order to derive a better age estimate from the CMD.

(2) We also determine cluster ages from applying recent isochrones that were not available previously.

(3) In addition, we derive metallicities for these clusters for the first time, using two different techniques.

(4) We have included an additional cluster that fell in the same CCD field as another cluster but was not previously analysed.

(5) Finally, we analyse the mean age and metallicity for the field population surrounding each cluster.

The work reported here follows the example of B98, who performed a more detailed analysis of a subsample of the G97 clusters lying in the outer disc. Here we have selected for study most of the remaining G97 clusters, in particular eight clusters, all but one of which lie in the inner disc of the LMC. Here we use the working definition we presented in B98: the inner disc is that region where the mean field turnoff becomes as bright as the clump, which occurs at a deprojected radius of ~4°. The lone outlier in our present sample is SL 549, which will be regarded as an outer disc cluster. We are aware of no other CMDs for any of these clusters or their surrounding fields, nor of any other age or metallicity determinations.

The cluster sample and the observations are described in Section 2. The construction of optimum CMDs is presented in Section 3. Ages and metallicities are derived in Section 4. In Section 5 we discuss our major results, and summarize our work in Section 6.

2 OBSERVATIONS AND REDUCTIONS

The subsample of G97 clusters studied in more detail here is delineated in Table 1, where we give the various star cluster designations from different catalogues, 1950 equatorial coordinates, galactic coordinates, and the approximate projected angular distance from the bar centre (taken as the position of the cluster NGC1928: $\alpha_{1950} = 5^h21^m19^s$, $\delta_{1950} = -69°31'30''$), which in turn is $\approx 0°.2$ south of the H I rotation curve centre (see Westerlund 1990, for a review of centroids). Finally, the last column of Table 1 lists deprojected angular distances R assuming that all clusters are part of the inclined disc, using the standard values given in Westerlund (1990). All but one of these clusters (SL 549) have deprojected radii from the LMC centre of $<4°$ and will therefore be referred to as 'inner disc' clusters. Note that SL678 lies in the same CCD field as SL 674 but was not studied by G97.

The observations were carried out with the CTIO 0.9m telescope in December, 1996 with the Tek2k #3 CCD, as described in G97. The scale on the chip is 0.40 arcsec per pixel, yielding an area 13.6×13.6 arcmin. The clusters were generally centred in the frames. The filters used were the Washington (Canterna 1976) *C* and Kron–Cousins *R* filters. The latter has significant throughput advantages over the standard Washington T_1 filter (Geisler 1996). As detailed in G97, we calibrated the observations to the C, T_1 system. In particular this filter combination allows us to derive accurate metallicities based on the standard giant branch technique outlined in Geisler & Sarajedini (1999).

Table 2 gives details of the observations. We spent no more than an hour total observing on any cluster. Airmasses ranged from ~1.2–1.4 and the seeing from 1.3–2.4 arcsec. All nights were of excellent photometric quality.

Table 1. Selected clusters.

Star cluster[a]	α [B(1950.0)]	δ [B(1950.0)]	l (deg)	b (deg)	r (deg)	R (deg)
SL 244	$05^h\ 07^m\ 49^s$	$-68°\ 36.3'$	279.4	−34.5	1.5	2.1
SL 359, KMHK 727	05 18 02	−68 31.5	279.1	−33.6	1.0	1.4
SL 446A, KMHK 858	05 24 36	−67 46.3	278.1	−33.2	1.8	2.0
SL 505, KMHK 960	05 29 36	−71 40.2	282.6	−32.1	2.3	2.9
SL 549, KMHK 1013	05 31 47	−64 16.5	273.8	−32.8	5.3	5.9
SL 555, LW 236, KMHK 1046	05 32 34	−72 10.8	283.1	−31.8	2.8	3.7
SL 674, ESO 86-SC26, KMHK 1281	05 43 18	−66 16.9	276.1	−31.5	3.8	3.9
SL 678, KMHK 1283	05 43 35	−66 12.5	276.0	−31.5	3.8	3.9

[a]Cluster identifications are from Shapley & Lindsay (1963, SL), Lyngå & Westerlund (1963, LW), Lauberts (1982, ESO) and Kontizas et al. (1990, KMHK).

Table 2. Observing log.

Date	Cluster	Filter	Exposure (s)	Airmass	Seeing ($''$)
1996 Dec. 11	SL 244	C	2100	1.36	1.8
		R	900	1.40	1.7
1996 Dec. 11	SL 359	C	2700	1.30	1.6
		R	900	1.31	1.3
1996 Dec. 13	SL 446A	C	2700	1.35	1.6
		R	900	1.38	1.5
1996 Dec. 11	SL 505	C	1500	1.37	2.4
		R	450	1.40	2.1
1996 Dec. 11	SL 549	C	2700	1.21	2.1
		R	900	1.21	1.8
1996 Dec. 11	SL 555	C	2100	1.36	2.1
		R	600	1.35	1.9
1996 Dec. 12	SL 674	C	2700	1.26	1.8
	SL 678	R	900	1.27	1.6

The data were reduced with the stand-alone version of DAOPHOT II and ALLSTAR (Stetson 1987) after trimming, bias subtraction and flat-fielding. More details on the observations, reductions and calibration procedures were given in G97. The final calibrated photometry for each cluster is available from the first author on request. Fig. 1 presents CCD images of the clusters.

3 ANALYSIS OF THE COLOUR–MAGNITUDE DIAGRAMS

3.1 Star clusters

One of the most important aspects to bear in mind in the analysis of LMC cluster CMDs is filtering out the unavoidable field contamination in order to more clearly delineate the fiducial cluster sequences. With this aim, we decided to build CMDs of stars distributed in different circular extractions centred on the clusters, and then to compare them in order to distinguish cluster features from those characterizing surrounding LMC fields. Notice that these inner disc clusters are in general embedded in very crowded fields (see Fig. 1). Thus, the task of selecting the size of the circular extraction represents a compromise between maximizing the number of stars necessary to define the fiducial cluster sequence and minimizing the contamination of field stars, and this is not as straightforward as desired. For this reason, we constructed for each cluster four CMDs from different annuli.

First, we determined the position of cluster centres by fitting Gaussians to the X and Y distributions of stars. Accuracy in the placement of these centres depended on (i) the ratio between the number of cluster and field stars, (ii) the sharpness of cluster star density profiles, and (iii) the intracluster fluctuations due to both cluster and field star density variations. We used the NGAUSSFIT routine of the STSDAS package to fit the projected X and Y star density distributions, and thus obtained cluster centre positions and full widths at half-maximum (FWHMs). Projected star distributions were sampled by counting the number of stars distributed in strips of 200 pixels wide along the X and Y directions across the clusters, respectively, with spatial resolutions of 5 and 10 pixels. These two different intervals were used to evaluate whether cluster positions changed with bin size. The result showed that the average position varied by less than 3 pixels.

Secondly, we used cluster FWHMs as a reference to define optimum circular extractions, once cluster positions were adopted. For this purpose, we also made use of the schematic finding charts drawn in Figs 1(a) and (b), where the sizes of the plotting symbols are proportional to the T_1 brightness of the stars. The radii of the smallest circular extractions were fixed to guarantee the presence of a predominant number of cluster stars over field stars in the extracted CMDs. However, these innermost extractions cannot contain the best representative sample of cluster stellar populations, due both to their small areas and increased crowding, but do minimize the influence of field stars. In contrast, the largest circular extractions allow us to trace mostly the surrounding fields. Finally, two additional intermediate circular extractions were used to obtain a better definition of the fiducial cluster sequences from a larger number of cluster stars, as well as to monitor the transition of cluster CMDs to a CMD dominated by field stars. The main criterion to define the intermediate radii was to choose those radii that allow us to see changes of the stellar population distribution in the CMDs. The choice of the various radii for each cluster was an iterative, somewhat subjective process designed to obtain the best representation of the cluster and its transition to the field. Figs 1(a) and (b) show the radii employed to define the 4 extractions for each cluster. The biggest circles were not included, since they encompass much larger areas than shown.

An example of the resulting set of extracted T_1 versus $C - T_1$ CMDs, for stars in the area of SL 674, is shown in Fig. 2. Panels in the figure give the extraction annuli in pixels. In most of the cluster fields, photometric limits (defined here crudely as the magnitude below which the number of photometered stars on the Main Sequence (MS) dramatically decreases due to measurement errors) for the innermost CMDs were brighter than those for more distant CMDs, due to the increasing crowding. The effect is most pronounced in the CMDs of SL 359, SL 446A, SL 555, SL 674 and SL 678, where the magnitude difference between the photometric limits of innermost and adjacent extracted CMDs reaches ≈ 1.0 mag. On the other hand, the larger photometric errors in the inner parts of the clusters provided by DAOPHOT do not differ from those in the surrounding field by more than 0.04 mag at any magnitude level. A more meaningful constraint on the quality of the photometry of the cluster core regions is given by measures of blended stars, which produce larger scatter in the fiducial cluster sequences.

The innermost extracted CMDs of the clusters show both of these crowding effects: the brighter limiting magnitude and/or the larger scatter than the adjacent extracted CMDs. The second and third radial region CMDs, although representative of outer cluster regions, still show the fiducial cluster sequences clearly.

After careful consideration of the various CMDs for each cluster, we decided to estimate the fundamental parameters of SL 244, SL 359, SL 505, SL 674 and SL 678 using the cluster main sequences (MSs) from the second radial region CMDs, while those for SL 446A, SL 549 and SL 555 were taken from the third radial region CMDs. Furthermore, since innermost extracted CMDs also contain valuable cluster information, in particular upper red giant branch (RGB) stars used to measure metallicity, we decided to include them together with such stars in the second or third extracted CMDs (whichever was not selected above) to obtain composite cluster CMDs. These composite CMDs – the MSs are from the above selected extracted CMDs and the RGB stars are from the innermost to the third extracted CMDs – are shown in Fig. 3, and were used to fit theoretical isochrones as well as to measure the δT_1 age index and the metal abundance.
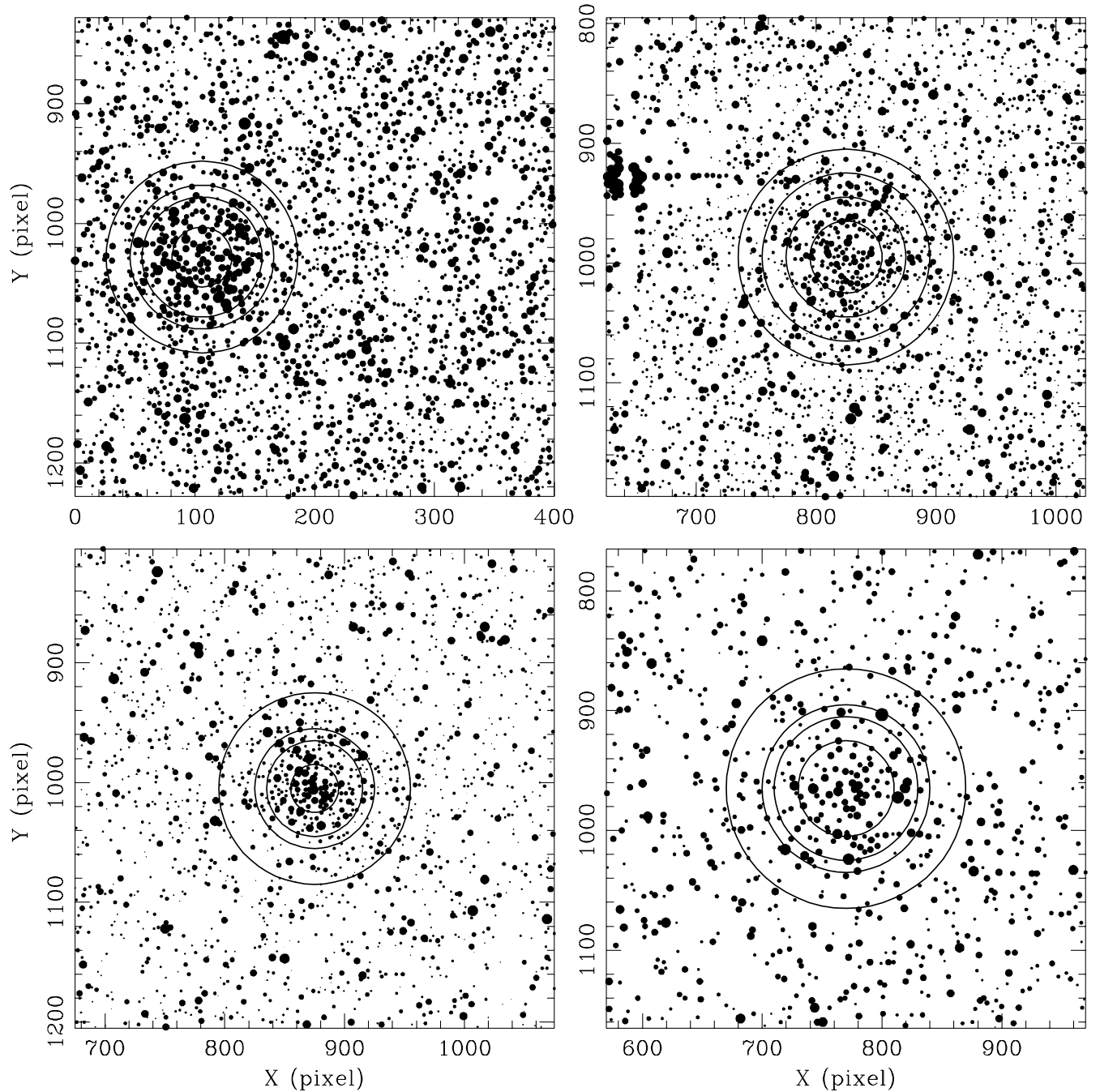
Figure 1. Schematic finding charts for the studied LMC cluster fields. (a) SL 244 (upper left), SL 359 (upper right), SL 446A (bottom left), and SL 505 (bottom right). (b) Sl 549 (upper left), SL 555 (upper right), SL 674 (bottom left), and SL 678 (bottom right). Four circular extractions are generally shown. North is up and east is to the left. The sizes of the plotting symbols are proportional to the T_1 brightness of the star.

3.2 Surrounding fields

The CMD of the surrounding field of a cluster was built from stars distributed within a region delimited by an inner circle centred on the cluster with a radius three times that of the cluster and extending to the boundary of the CCD field. For this purpose, we defined the radius of a cluster as the distance from its centre at which the number of stars per arcmin^2 above the background level equals $4 \times \sigma_{back}$, where σ_{back} represents the standard deviation of the star density in the surrounding field. The background level and dispersion were determined from the cluster radial profile obtained by counting the number of stars from the cluster centre outwards within rings of 5 pixels. This limiting circle statistically constrains the contamination of cluster stars in the field CMDs to be less than 5 per cent of the cluster stars. In the case of the fields of SL 244, SL 446A, and SL 674/SL 678, other clusters were observed in the same images, and we also excluded them from the surrounding fields following the same procedure. The resulting CMDs are shown in Fig. 4, which also shows the reddening vector corresponding to $E(C - T_1) = 1$ mag.
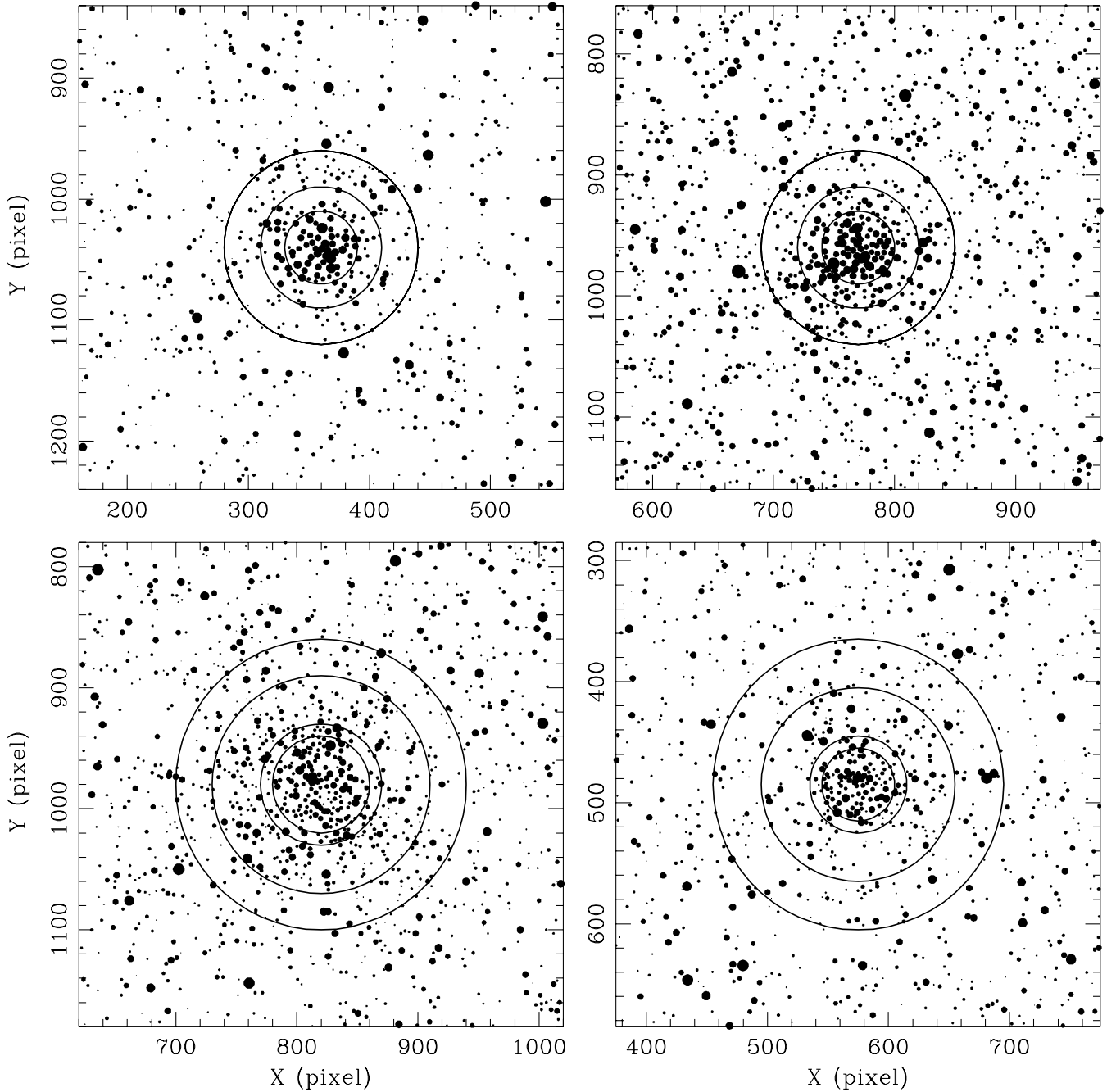
Figure 1 – *continued*

Fig. 4 shows that a mixture of different stellar populations is present in each field. MSs are well populated and extend for many magnitudes. Different limiting magnitudes are also visible as expected from the different crowding and exposure times, particularly in the C filter. Assuming that MSs come from the superposition of MSs with different TOs, they appear to be dominated by a 1–3 Gyr old population as deduced from the δT_1 index, which measures the difference in magnitude between the mean magnitude of the clump and the MSTO (G97). We also estimated an upper age limit of $\sim$4–7.5 Gyr using the δT_1 index, depending on the observed limiting magnitude. This significant age range is also supported by the presence of broad subgiant branches due to the transition of MS stars with different ages to the giant branch. RGBs are also clearly visible, covering a wide range in colour from $C - T_1 \sim 1.5$ up to 4.

A more detailed examination of the RGBs allows us to draw the following conclusions: first, the observed LMC fields appear not to be affected by differential reddening, since differential reddening would produce tilted red clumps (RCs) following the reddening vector. Secondly, the different colour spreads of the RCs show that age/metallicity ranges change from field to field. Indeed, the $C - T_1$ colour spread of the RCs varies from $\Delta(C - T_1) \approx 0.5$ up to 0.8 for SL 674/SL 678 and SL 505, respectively. Furthermore, the larger the measured colour range, the younger the dominant population in a field. Thirdly, we only detected vertical structure (VS) stars in the field of SL 549. VS stars were conclusively identified by Piatti et al.
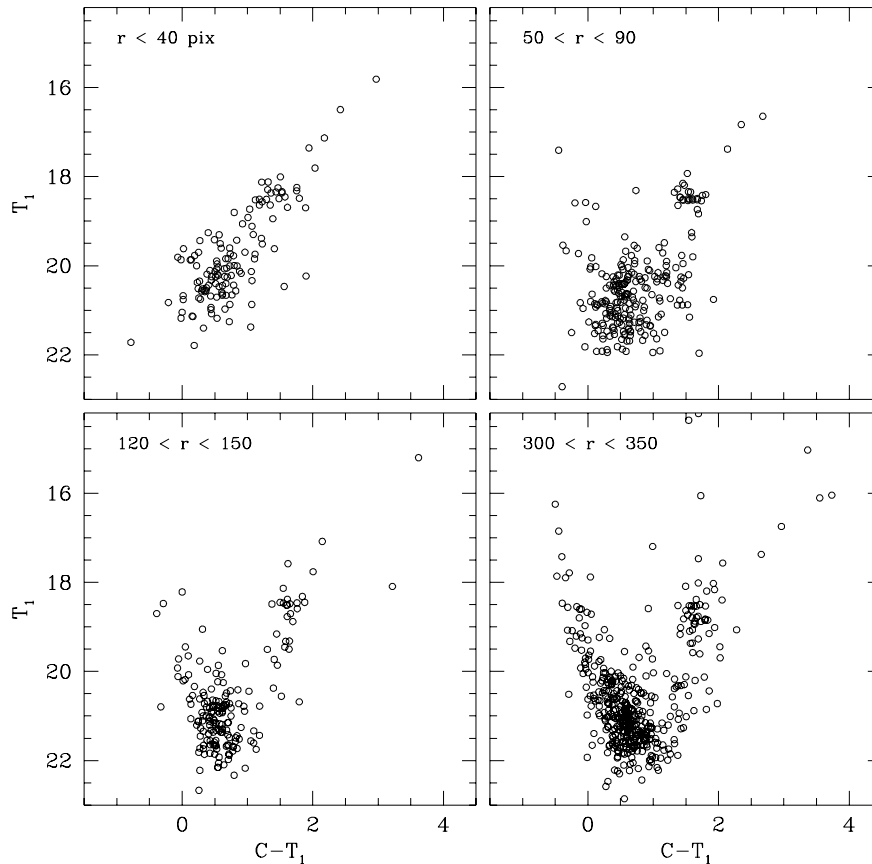
Figure 2. Washington T_1 versus $C - T_1$ CMDs of stars in the field of SL 674. Extraction radius in pixels is given in each panel.

(1999) as a group of stars that lie below the RC at its bluest colour and up to 0.45 mag fainter. We counted the number of stars in the VS and RG boxes, according to Piatti et al. (1999) prescriptions, and found 58 and 1064 stars, respectively. These values are in very good agreement with the position of VS LMC field stars in their fig. 5. The existence of VS stars in the surrounding field of SL 549 suggests that it contains a significant number of 1–2 Gyr old stars with metallicities higher than [Fe/H] ≈ -0.9 dex, whose masses are slightly higher than those of fiducial RC stars, as clearly shown by the isochrones of Girardi et al. (2000). Note that SL 549 is the most distant cluster from the LMC centre that we observed.

4 AGES AND METALLICITIES

We derived ages and metallicities using two independent techniques for each parameter. First, we estimated ages of the cluster sample by fitting theoretical isochrones computed by Lejeune & Schaerer (2001) to the cluster CMDs. Lejeune & Schaerer calculated for the first time isochrones for the Washington system, using an updated version of the empirically and semi-empirically calibrated *BaSel* library of synthetic spectra (Lejeune, Cuisinier & Buser 1997, 1998; Westera, Lejeune & Buser 1999). Thus, we could determine cluster ages without transforming isochrones from the *UBVRI* to the CMT_1T_2 system, as was required previously. To enter these isochrones in the cluster CMDs, we first adopted cluster reddenings and an LMC distance modulus. Cluster reddening values were estimated by interpolating the extinction maps of Burstein & Heiles (1982, hereafter BH). BH maps were obtained from H I (21-cm) emission data for the southern sky and provide us with foreground

$E(B - V)$ colour excesses which depend on the Galactic coordinates. More recently, Schlegel, Finkbeiner & Davis's (1998, hereafter SFD) obtained full-sky maps from 100-μm dust emission. They found that at high-latitude regions, the dust map correlates well with maps of H I emission, but deviations are coherent in the sky and are especially conspicuous in regions of saturation of H I emission towards denser clouds and of formation of H_2 in molecular clouds. Since the $E(B - V)_{SFD}$ values for our clusters are 5–10 times higher than the $E(B - V)_{BH}$ values for these inner disc clusters, the SFD values are assumed to be saturated and we used the BH values. Our clusters do not lie in any obvious dust patches, as shown on either our frames, the DSS or the Hodge Atlas. Table 3 lists the BH $E(B - V)$ colour excess for each cluster. We used a true distance modulus for the LMC of $(m - M)_0 = 18.50 \pm 0.10$, the consensus obtained recently from several investigations using the K-band magnitude of the RC (Alves et al. 2002; Sarajedini et al. 2002; Pietrzynski & Gieren 2002).

We then selected a set of isochrones computed taking into account overshooting effects and superimposed them on the cluster CMDs, once they were properly shifted by the corresponding $E(B - V)$ colour excess and LMC apparent distance modulus. Fig. 5 shows the results of the fittings. For each cluster we plot two different isochrones with ages and metallicities bracketing the derived value; while columns 3 and 6 of Table 3 list the adopted cluster parameters. Cluster ages were determined from a weighted average of the ages of isochrones which best matched the shape and position of cluster MSs, particularly at the TO level, as well as the T_1 magnitude of the RC. We also similarly estimated metallicities from the isochrones by comparing them to the RGBs. We noted,
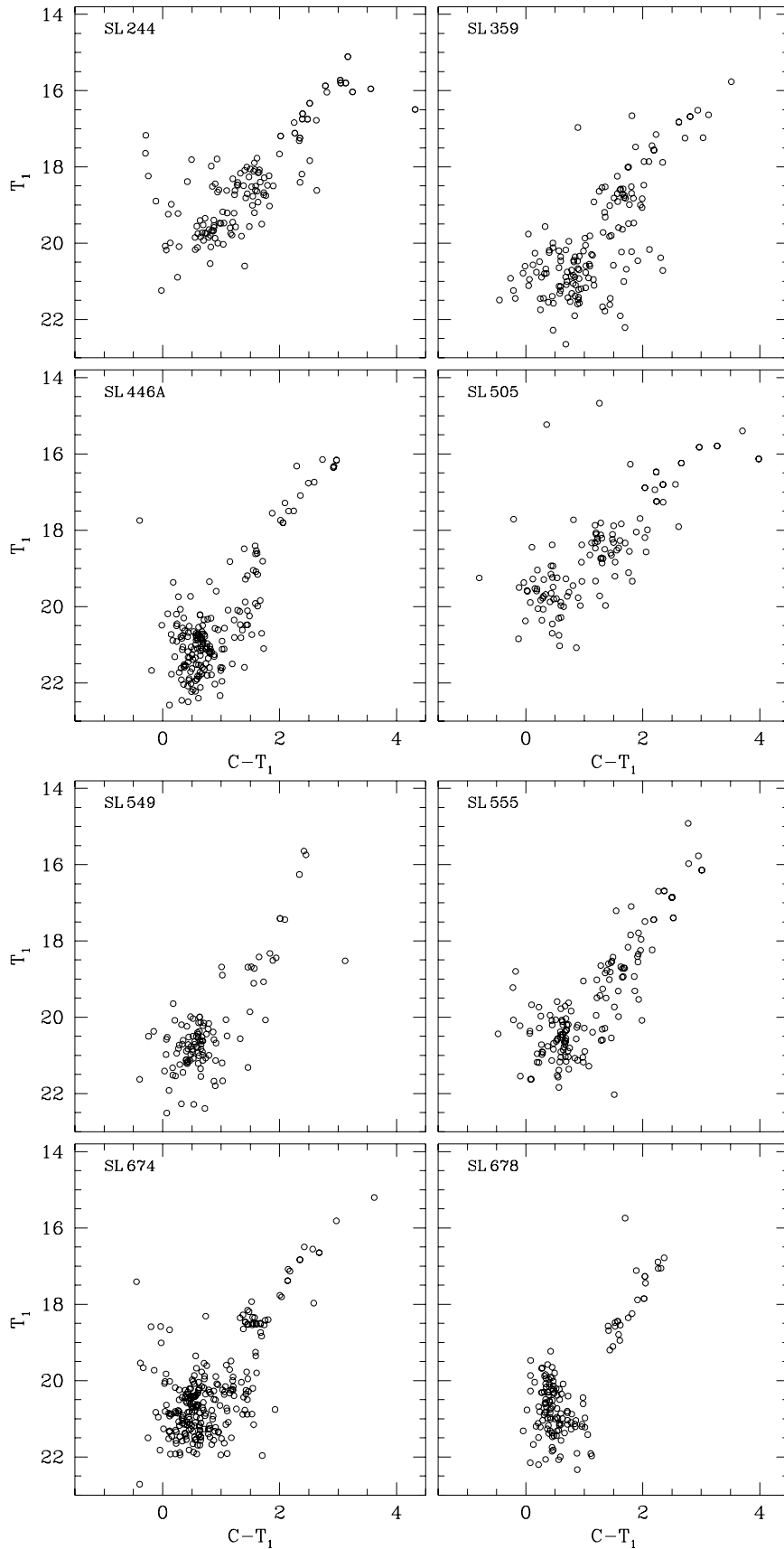
Figure 3. Composite Washington T_1 versus $C - T_1$ CMDs of stars in the fields of the studied clusters. These are the diagrams used to derive cluster parameters. (a) SL 244 (upper left), SL 359 (upper right), SL 446A (bottom left), and SL 505 (bottom right). (b) Sl 549 (upper left), SL 555 (upper right), SL 674 (bottom left), and SL 678 (bottom right).
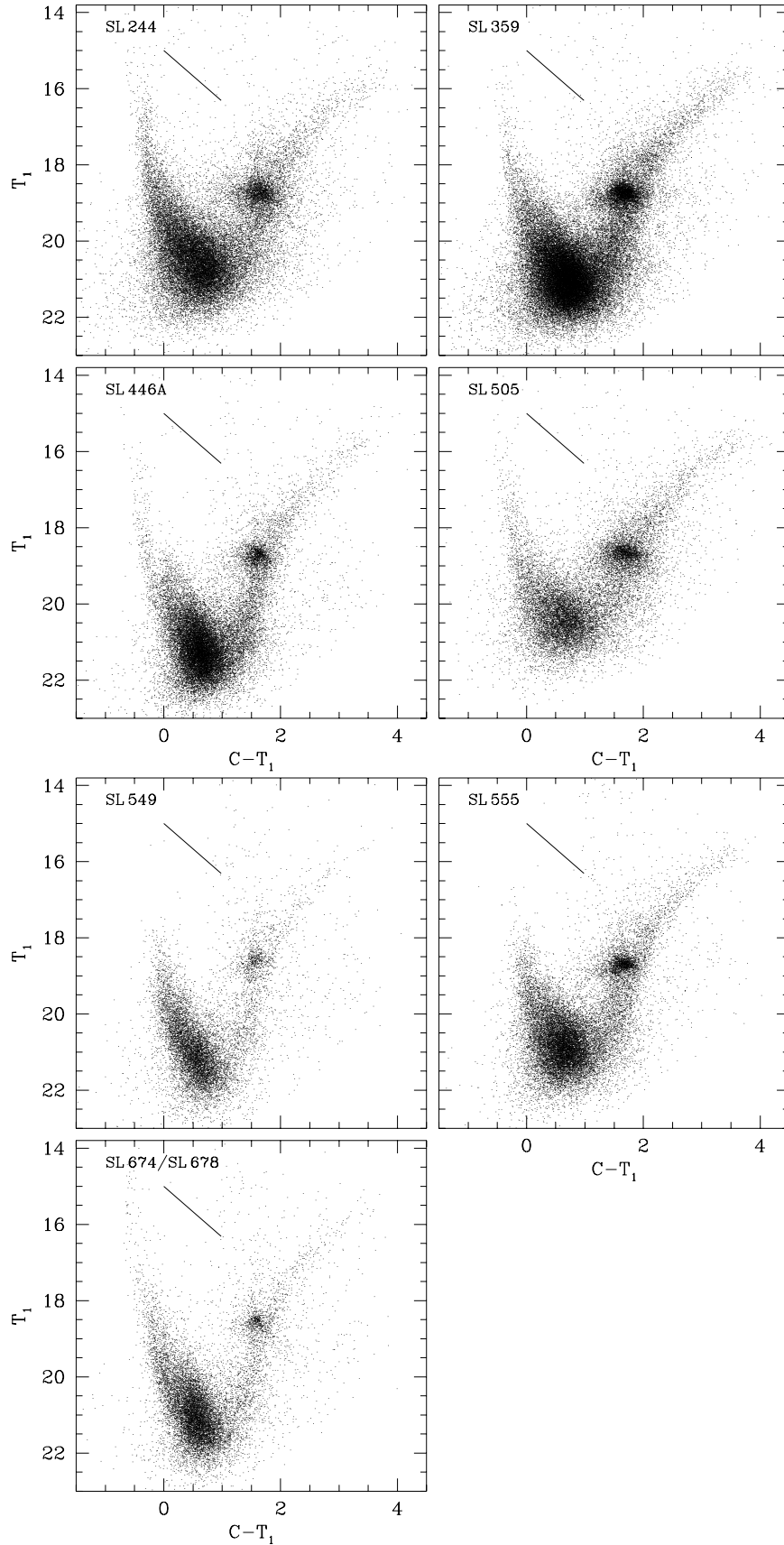
Figure 4. Washington T_1 versus $C - T_1$ CMDs of stars in the surrounding fields of the studied clusters. (a) SL 244 (upper left), SL 359 (upper right), SL 446A (bottom left), and SL 505 (bottom right). (b) Sl 549 (upper left), SL 555 (upper right), SL 674/678 (bottom left). A reddening vector corresponding to $E(C - T_1) = 1$ mag. is shown in each case.

Table 3. Reddenings, ages and metallicities of LMC clusters.

Name	$E(B-V)$	Isochrone age (Gyr)	δT_1	δT_1 age (Gyr)	Isochrone [Fe/H]	SGB [Fe/H]
SL 244	0.06	1.3 ± 0.3	1.10 ± 0.2	1.5 ± 0.3	-0.7 ± 0.2	-0.75 ± 0.3
SL 359	0.06	1.6 ± 0.4	1.60 ± 0.2	2.0 ± 0.3	-0.4 ± 0.2	-0.45 ± 0.3
SL 446A	0.06	2.2 ± 0.5	1.85 ± 0.2	2.4 ± 0.4	-0.9 ± 0.2	-0.75 ± 0.3
SL 505	0.07	0.9 ± 0.2	1.15 ± 0.2	1.5 ± 0.3	-0.5 ± 0.2	-0.7 ± 0.3
SL 549	0.04	2.0 ± 0.5	1.60 ± 0.2	2.0 ± 0.3	-0.9 ± 0.2	–
SL 555	0.07	1.6 ± 0.5	1.50 ± 0.2	1.8 ± 0.3	-0.7 ± 0.2	-0.75 ± 0.3
SL 674	0.05	2.0 ± 0.4	1.80 ± 0.2	2.3 ± 0.3	-0.9 ± 0.2	-0.8 ± 0.3
SL 678	0.05	1.5 ± 0.3	1.60 ± 0.2	2.0 ± 0.3	-0.8 ± 0.2	-0.8 ± 0.3

however, that the theoretically computed bluest stage during the He-burning core phase is redder than the observed RCs, a behaviour which has also been detected in other independent earlier studies of Galactic open clusters (Clariá et al. 1994; Rosvick 1995). A similar result was found by Meynet, Mermilliod & Maeder (1993) from the fitting of isochrones in the M_V versus $(B-V)_o$ diagram. However, Mermilliod et al. (2001) found excellent agreement between theory and observation for the RCs of intermediate age clusters (IACs).

We also derived ages from the δT_1 index, calculated by determining the difference in the T_1 magnitude of the RC and MSTO in cluster CMDs. We assigned to the TO T_1 magnitude an uncertainty twice that typical of the photometry at the TO level, i.e. $\langle \sigma_{TO} \rangle = 0.10$ mag. Given the crowded nature of these fields, the rather sparse RCs in some cases, photometric errors near the MS, etc, and especially the somewhat subjective nature of this procedure, significant errors may result. In order to address these, both DG and AEP determined independent δT_1 values for all clusters. Finally, since δT_1 values have already been derived for these clusters in G97 (from CMDs where field star contamination was presumably somewhat more problematic), we used the mean of these three determinations as our final value, which is given in Table 3. Note that this procedure effectively gives double weight to the present CMDs. All three assessments were generally in good agreement (total spread of 0.1–0.5 in δT_1, with a mean spread of 0.3) except for 1 cluster where, upon careful inspection, it became clear that the G97 value was spurious and was not used in the mean. The DG and AEP values differed by 0.2 in the mean, with DG values being uniformly larger. We estimate that the δT_1 mean values should be accurate to about 0.2.

We then derived ages from the mean δT_1 values using equation (4) of G97 and these are also presented in Table 3. A typical error is ± 0.3 Gyr. Since TOs were measured from the brightest part of the TO regions, the ages should be considered as lower limits to the cluster ages. The present values should be preferred over those given in G97.

Comparing the isochrone and δT_1 ages, we find that the latter are generally slightly larger, with a mean difference of 0.3 Gyr. In only one case is the difference more than 0.5 Gyr. This is certainly good agreement given the respective errors. Note that none of our sample have a published age or metallicity estimate (besides G97).

Representative ages for cluster surrounding fields were also estimated by measuring δT_1 indices in Fig. 4. Since field CMDs are composed of MSs of different stellar populations, we derived δT_1 values for the MS with the TO containing the largest number of stars. We assumed that the observed MS is the result of the superposition of MSs with different TOs (ages) and constant luminosity functions. Hence, the difference between the number of stars of two adjacent magnitude intervals gives the intrinsic number of stars belonging to the faintest interval. Consequently, the biggest difference is directly

related to the most populated TO. To find this biggest value, we counted the number of stars in bins of 0.5 mag along field MSs, which we delimited by lower and upper envelopes defined by the expressions:

$$T_1 = 6 \times (C - T_1) + 20$$

and

$$T_1 = 6 \times (C - T_1 - 0.5) + 20,$$

respectively. The calculated δT_1 values with their uncertainties and the derived LMC field ages are listed in Table 4.

Finally, metallicities for the cluster sample and their surrounding fields were also obtained using the $[M_{T_1}, (C - T_1)]$ plane with the standard giant branches (SGBs) of Geisler & Sarajedini (1999). They demonstrated that the metallicity sensitivity of the SGBs (each giant branch corresponds to an isoabundance curve) is three times higher than that of the V, I technique (Da Costa & Armandroff 1990) and that, consequently, it is possible to determine metallicities three times more precisely for a given photometric error. However, the SGBs were defined for [Fe/H] < -0.5 using globular clusters older than 10 Gyr. In view of the well known age – metallicity degeneracy, it is important to examine as closely as possible the effect of applying such a calibration based on very old objects to much younger IACs. B98 explored this effect empirically by comparing SGB-based metallicities for 11 IACS to standard values. They found a relatively constant offset of ~ 0.4 dex, in the sense expected: that the SGB metallicities were underestimated due to the effects of age for clusters younger than ~ 3 Gyr. B98 and subsequent papers in this series have incorporated this rough correction into their SGB metallicity estimates for IACs.

We now have the means at our disposal to investigate this effect in much more detail thanks to the recent publication of isochrones in the Washington system by Lejeune & Schaerer (2001). We proceed as follows: we employ the $z = 0.001$ and 0.004 isochrones to derive $(C - T_1)_0$ at $M_{T_1} = -1.5$ ($z = 0.004$) and -2 ($z = 0.001$) for a variety of ages from 1–10 Gyr. We then determine the difference in $(C - T_1)_0$ between the 10 Gyr isochrone and the isochrones for other ages at the same metallicity. We next use the metallicity calibration for the SGB technique from Geisler & Sarajedini (1999) to translate this difference in colour into a difference in metallicity, using the linear metallicity calibrations at each M_{T_1}. This then gives the theoretically predicted metallicity correction due to age and should be especially useful as we are using the isochrones differentially. These are the lines shown in Fig. 6.

Next we compare these theoretical predictions with the empirical offsets found by B98 for 11 clusters. We have taken the standard metallicities and ages from the best available sources for each cluster. These are displayed as the squares in Fig. 6. Except for one cluster, the agreement between the $[z = 0.004$ ([Fe/H] ~ -0.7), $M_{T_1} = -1.5]$ prediction and observations is quite good and gives
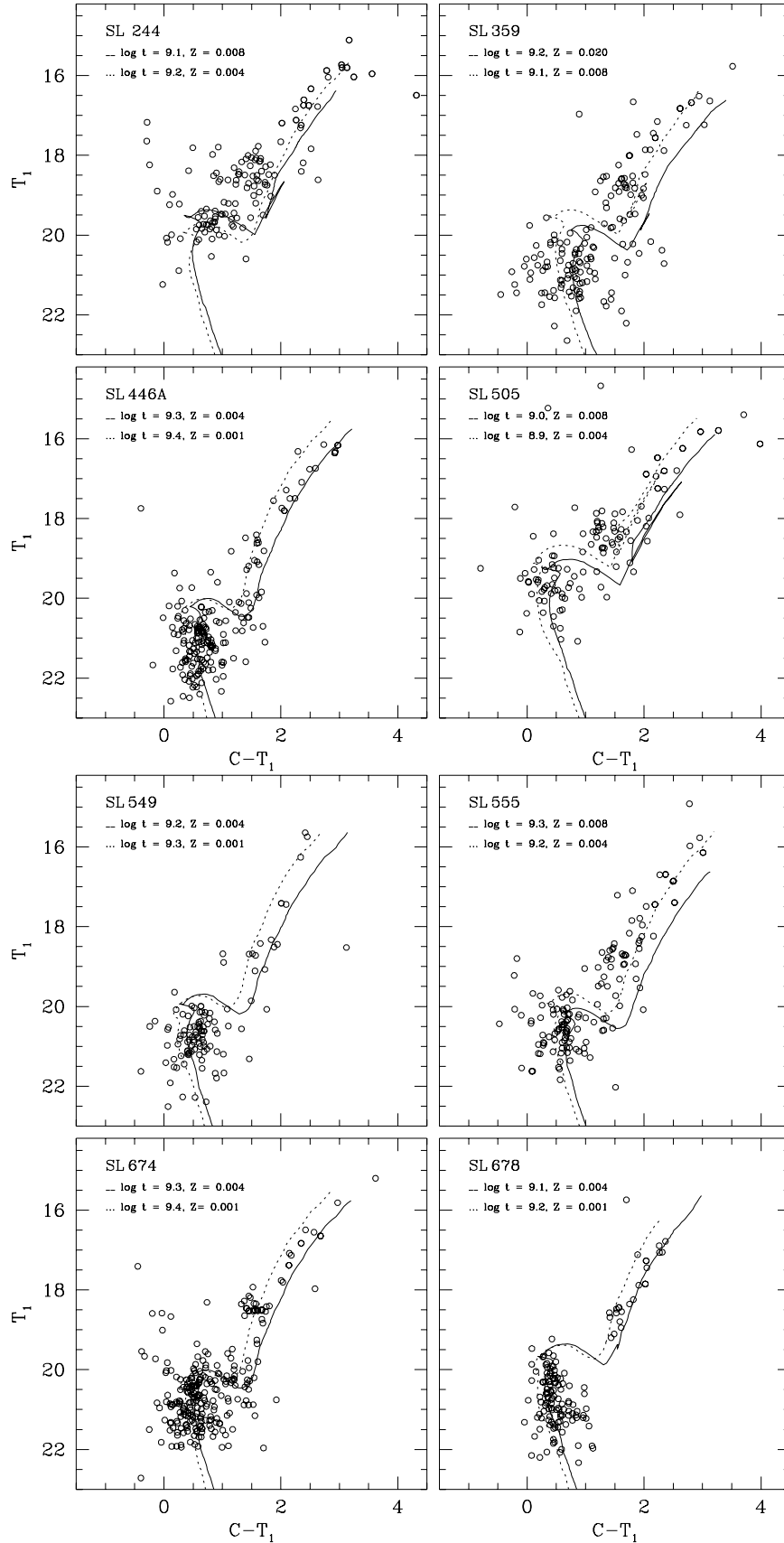
Figure 5. Washington T_1 versus $C - T_1$ CMDs for the clusters. Isochrones from Lejeune & Schaerer (2001), computed taking into account overshooting, are overplotted. (a) SL 244 (upper left), SL 359 (upper right), SL 446A (bottom left), and SL 505 (bottom right). (b) Sl 549 (upper left), SL 555 (upper right), SL 674 (bottom left), and SL 678 (bottom right).

Table 4. Ages and metallicities of LMC cluster surrounding fields.

Name	δT_1	δT_1 age (Gyr)	SGB [Fe/H]
SL 244	0.8 ± 0.1	1.3 ± 0.1	-0.3 ± 0.3
SL 359	1.3 ± 0.1	1.6 ± 0.1	-0.4 ± 0.3
SL 446A	2.3 ± 0.1	3.9 ± 0.4	-0.8 ± 0.3
SL 505	0.9 ± 0.1	1.3 ± 0.1	-0.3 ± 0.3
SL 549	1.9 ± 0.1	2.5 ± 0.2	-0.7 ± 0.3
SL 555	1.8 ± 0.1	2.3 ± 0.2	-0.55 ± 0.3
SL 674/678	2.0 ± 0.1	2.8 ± 0.3	-0.8 ± 0.3

us confidence in this procedure. We then adopt this theoretical prediction (shown as the solid line) as the correction to be applied to our SGB metallicities as a function of age.

We then followed the standard SGB procedure of entering absolute M_{T_1} magnitudes and intrinsic $(C - T_1)_o$ colours for each cluster and field into fig. 4 of Geisler & Sarajedini to obtain by interpolation metal abundance values ([Fe/H]) to which we added the appropriate age correction, using the δT_1 ages we derived. The derived metallicities for clusters and surrounding fields are listed in the last column of Tables 3 and 4, while Fig. 7 illustrates the position of the cluster RGBs in the $[M_{T_1},(C - T_1)]$ plane. Note that the field RGBs are very well populated in general and show a significant colour spread at a given magnitude, implying either a spread in age, metallicity or both. Here we have simply given the mean metal abundance derived from the above analysis. The very limited number of upper giant branch stars in SL 549 (5) and their wide implied metallicity spread prevented us from deriving a useful metallicity. For the other clusters and their surrounding fields we could determine mean metallicities to about 0.3 dex including all error sources. Note that due to the steepness of the age correction for the youngest clusters (<1.5 Gyr), a given age error will result in a larger metallicity error and will bias the resulting metallicities upwards.

The age-corrected SGB metallicities are compared to the isochrone metallicities for our clusters in Fig. 8. In general, the two metallicity estimates agree very well, further supporting our
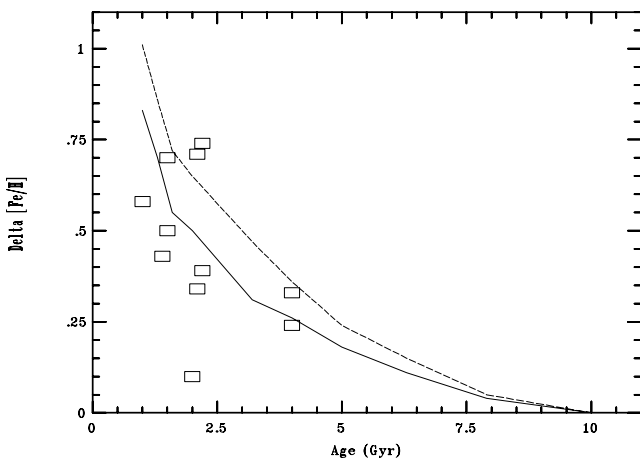

Figure 6. Derivation of the metallicity correction, Delta [Fe/H], needed for IACs due to their much younger ages than for the original SGB calibrating clusters. The lines show the theoretical predictions derived from the Lejeune and Schaerer (2001) isochrones for two different metallicities and M_{T_1} levels. The solid line is for [Fe/H]$= -0.7$ and $M_{T_1} = -1.5$ and is our adopted correction curve. Squares show 11 clusters studied in B98 with well known metallicities used to calibrate the age offset. The observed clusters reproduce the solid line well, supporting our adoption of this theoretical prediction to correct SGB metallicities for the age effect.

age-correction procedure. The mean difference for the 7 clusters in common is only 0.01 ± 0.11 dex. In the following, we will adopt the isochrone-based metallicities since all of these clusters are IACs and therefore require large age corrections for the SGB procedure. Note that this correction is a full 0.5 dex at 2 Gyr and still a significant 0.18 dex for a 5 Gyr object. Also note that the previously-recommended correction procedure – no correction for clusters older than 5 Gyr, a constant 0.2 dex correction for objects between 3 and 5 Gyr, and 0.4 dex for objects younger than 3 Gyr – is both too simplistic and generally an underestimate of the age effects, especially for clusters younger than 2 Gyr. We recommend the following procedure for future SGB metallicity determinations in the Washington system: first estimate the age and standard SGB metallicity and then use the solid line given in Fig. 6 to correct the SGB metallicity for objects older than 2 Gyr. For younger objects, use the isochrone-based metallicity.

Finally, a simple comparison between the derived δT_1 ages and SGB metallicities of clusters and surrounding fields shows that the clusters are on average 0.3 ± 0.6 Gyr younger and 0.18 ± 0.21 dex more metal-poor than their respective fields. Neither difference appears significant.

5 ANALYSIS

We here present an analysis of the most salient features of our cluster sample. Note that these 8 clusters all lie within the narrow age range of $\sim$1.5–2.5 Gyr. Following G97 and B98, we will refer to these as IACs, covering the age range from 1–3 Gyr. We will also include the corresponding fields.

First, it is of some interest to search for any metallicity gradient in the LMC disc, given that the Galaxy has long been known to possess such a gradient (e.g. Janes 1979; Friel & Janes 1995; Piatti, Clariá & Abadi 1995). Since our current sample is mostly confined to the inner disc, we supplement these clusters with those studied in an identical manner in B98 (with the exception of ESO 121-SC03 (age $\sim$9 Gyr) which we discard, as all other clusters are IACs), which cover a much larger radial range. However, before we can do this, we first apply the above-derived age correction to the SGB metallicities derived by B98 so that they are on the same corrected metallicity scale as our sample. We can then combine the samples. Fig. 9 demonstrates that no metallicity trend with radius is seen in either the clusters or their surrounding fields. This supports previous negative results obtained by Olszewski et al. (1991) and B98. However, we note that Cole (2002) has uncovered several hints of an overall gradient from studies of the 2MASS data base of LMC field stars and further studies are warranted.

We next examine more closely the slight mean metallicity difference obtained above between the clusters and their fields. Notably, B98 obtained a very similar result, finding that the metallicity of their sample of 14 IACs averaged 0.12 dex more metal-poor than the corresponding field. Our reanalysis of their sample yields a mean difference of 0.08 ± 0.17 dex (standard deviation) in the same sense. For the combined sample of 21 objects, we find that the clusters average -0.60 ± 0.19 and the fields -0.48 ± 0.17, with a mean difference of 0.12 ± 0.15 dex for the 17 objects with both cluster and field metallicities. This offset can be seen in Fig. 9, where the field points generally lie slightly above the clusters. This difference is however not statistically significant. Note that the clusters are, if anything, slightly younger than their fields. The fact that the slight metallicity difference persists for both samples is intriguing, although the difference is certainly within the errors. There is no other evidence that we are aware of for or against the presence of such a difference from other studies.
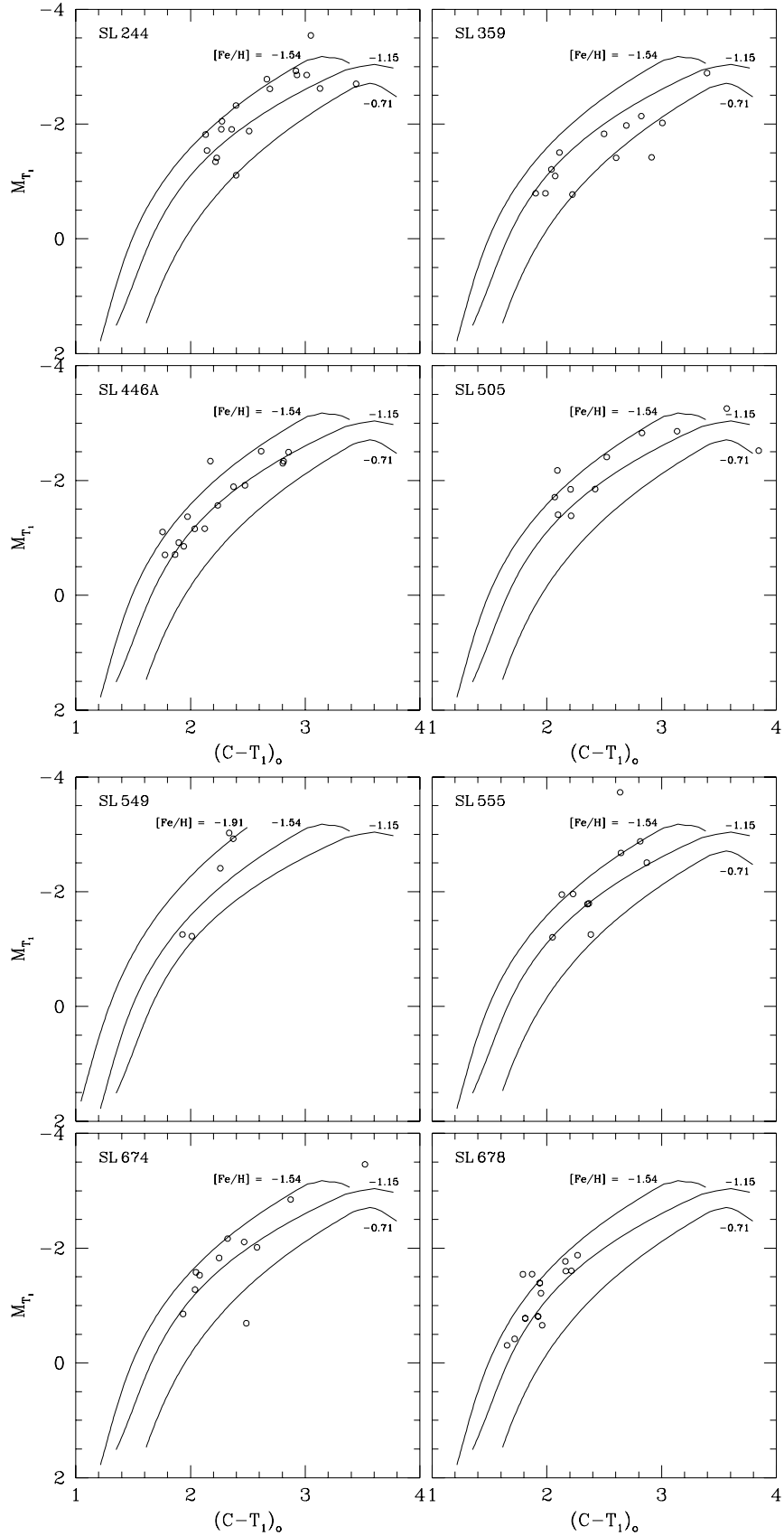
Figure 7. Washington M_{T_1} versus $(C - T_1)_o$ diagram of upper RGB stars in the studied clusters, with standard giant branches from Geisler & Sarajedini (1999) superimposed. Note that an age-dependent correction to the indicated metallicities, as derived in the text, was applied for these clusters. (a) SL 244 (upper left), SL 359 (upper right), SL 446A (bottom left), and SL 505 (bottom right). (b) Sl 549 (upper left), SL 555 (upper right), SL 674 (bottom left), and SL 678 (bottom right).
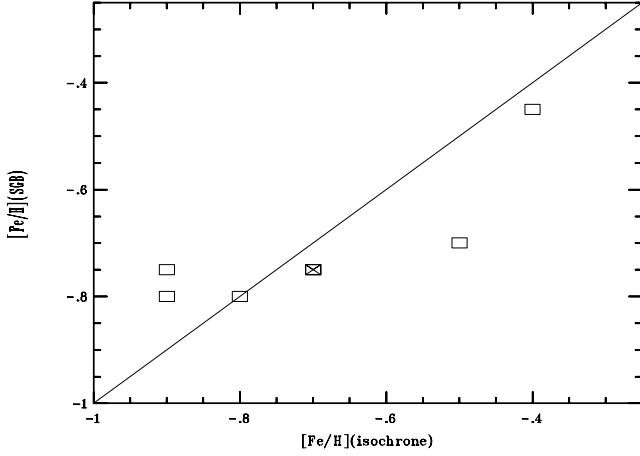
Figure 8. SGB metallicity versus isochrone metallicity for our cluster sample. An X inside a square indicates two clusters superimposed. The line shows perfect agreement. In general, the two metallicity estimates agree very well.
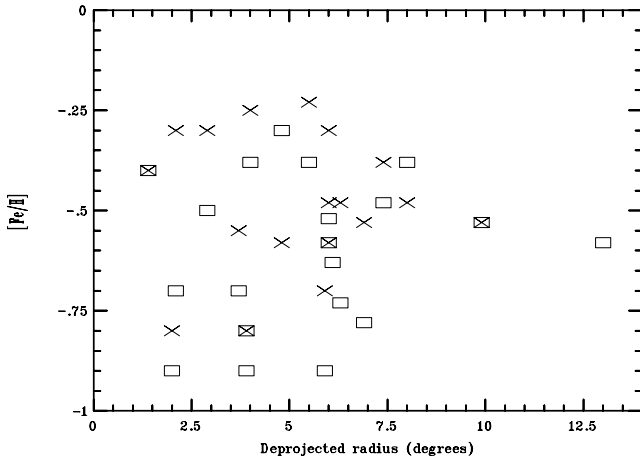
Figure 9. Metallicity versus deprojected radius from the centre of the LMC, for both clusters (squares) and their surrounding fields (X's), for all objects studied here and in B98 with ages between 1–3 Gyr.

B98 found that the IACs in their sample had a mean metallicity of -0.66 and averaged 0.24 dex more metal-poor than IACs in the Olszewski et al. (1991) sample, and argued that the difference was not due to different metallicity scales, since clusters in common gave similar abundances. Our combined sample now yields a mean metallicity of -0.60, 0.2 dex more metal-poor than the IACs in Olszewski's sample, which have a mean of -0.40 ± 0.21. Our Washington metallicities are now in slightly better agreement with those of Olszewski et al. for IACs – the difference found by B98 was due in part to underestimating the age effect. However, an offset still remains.

Beasley, Hoyle & Sharples (2002) recently derived ages and metallicities for 24 LMC clusters from fitting SSP models to integrated spectra. We have no IACs in common, but for the 4 IACs in common with Olszewski et al., the Beasley et al. metallicities average 0.19 ± 0.22 dex more metal-poor. Secondly, for their 9 IACs, Beasley et al. find a mean metallicity of -0.71 ± 0.26 dex, 0.1 dex more metal-poor than our mean and 0.3 dex lower than found by Olszewski. This latter difference appears significant. We note that our mean is in between those of the two other studies. In view of the small sample size of the Beasley IAC sample, we will
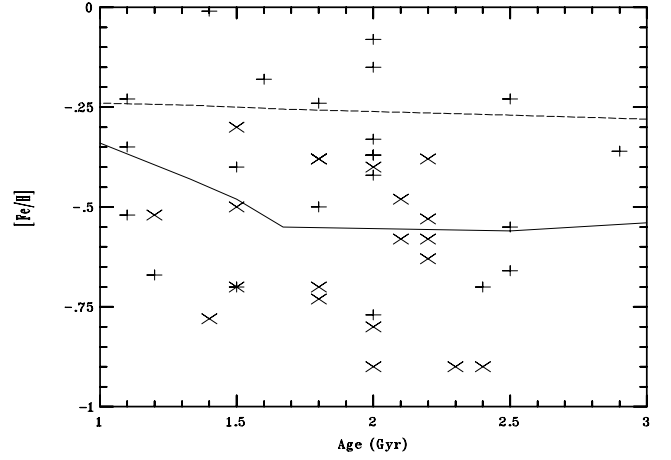

Figure 10. Metallicity versus age for IACs, including objects studied using the Washington system (X's) and Ca II triplet spectra of individual stars from Olszewski et al. (1991 − +'s). The curves are models from Pagel & Tautvaiŭienė (1998) for a continuous star formation rate (dashed) and a 3-Gyr burst (solid). IACs are found to have a very uniform mean metallicity and metallicity spread and are in good agreement with the burst model.

restrict ourselves in the following to metallicities derived here and from Olszewski. However, we note three recent studies indicating lower abundances may be correct. The metallicity distribution for 39 field stars derived by Cole et al. (2000) has a mean of -0.64, although these may include a number of older stars, the metallicities of which would be expected to be somewhat lower. Secondly, Hill et al. (2000) high resolution spectroscopic analysis of two giants in the IAC NGC 1978 found [Fe/H] ~ -1 instead of the value of ~ -0.4 found by both Olszewski et al. and Beasley et al. Thirdly, in an integrated spectra study similar to that of Beasley et al., Leonardi & Rose (2002) find their sample of 15 IACs to be 0.26 ± 0.34 dex more metal-poor than Olszewski's values.

Fig. 10 illustrates the age–metallicity relation for IACs from both the present sample (plus B98) and Olszewski et al. We have used the ages derived in the relevant paper, except we have used ages from Beasley et al. for a few IACs for which Olszewski had metallicities but no ages available. A total of 42 IACs are included. The clusters all lie within [Fe/H] ~ -0.9 to solar. The mean metallicity (–0.50) and its spread (0.23 dex) are very constant in this range. In addition we plot the continuous star formation rate (dashed curve) and 3-Gyr burst (solid curve) age–metallicity relations predicted by the models of Pagel & Tautvaiŭienė (1998). The burst model clearly provides a good fit to the cluster data, much better than the continuous model. The mean metallicity predicted, at least from 1.5–3 Gyr, is very similar to that observed. However, the burst model does predict a significant increase in the metallicity due to the burst, starting around 1.7 Gyr ago. There may be a slight increase in the data: comparing the mean metallicities for clusters older and younger than this value, we find the younger clusters are 0.07 dex more metal-rich than the older clusters, but the spread remains constant at 0.23 dex. We will defer to another paper (Piatti et al., in preparation) a more detailed analysis of the age–metallicity relation for our full sample of clusters analysed with the Washington system, including younger clusters, where the increase in metallicity for such clusters predicted by the bursting model is indeed observed.

6 SUMMARY

This paper continues our series of studies of the star clusters of the LMC using Washington photometry. In this contribution, we present

Washington system colour–magnitude diagrams for 8 star clusters and their surrounding fields which, with one exception, lie within the inner parts of the LMC disc. These clusters were (mostly) studied originally by G97 and had preliminary ages derived for them. Other than this study, no previous efforts to investigate the ages and/or metallicities of these clusters have been published. We have considerably improved our original analysis of these clusters in a number of ways. First, careful attention is paid to separating out the cluster and field star distributions, which are particularly important for these crowded fields. Ages and metallicities are then determined in a consistent manner for both the cluster and field star populations employing two different techniques. We compare the CMDs with theoretical isochrones in the Washington system and we also derive ages using the magnitude difference between the red clump and the turnoff, and derive metallicities by comparing the giant branches to standard calibrating clusters. For this latter technique we significantly improve the required age correction based on a comparison of the isochrones and observed clusters. The two methods for determining both ages and metallicities are in good agreement with each other.

The clusters all have δT_1 ages in the narrow range from 1.5 to 2.5 Gyr, and are thus intermediate age. Metallicities range from -0.4 to -0.9. We find that the stellar population of each star cluster is generally quite similar to that of the field where it is embedded, sharing its mean age and metallicity. Combining the present sample with a revision of that of Bica et al. (1998) studied similarly, we find no evidence for a metallicity gradient. We compare our mean metallicities for IACs with those derived by Olszewski et al. (1991) and Beasley et al. (2002) using different techniques. The revised age correction has now brought our results into slightly better agreement with those of Olszewski et al., alleviating some of the difference found previously by B98; however, there remains an offset. The Beasley et al. metallicities are lower than ours and significantly lower than those of Olszewski. Combining our sample with Olszewski's, we investigate the age–metallicity relation for 42 IACs. This shows that LMC clusters formed between 1–3 Gyr ago with a mean metallicity (–0.5 dex) and metallicity spread (0.23 dex) independent of age. Good agreement is found with the burst model of Pagel & Tautvaišienė (1998).

ACKNOWLEDGMENTS

REFERENCES

Alves D. R., Rejkuba M., Minniti D., Cook K. H., 2002, ApJ, 573, L51
Bica E., Geisler D., Dottori H., Clariá J. J., Piatti A. E., Santos J. F. C., Jr, 1998, AJ, 116, 723 (B98)
Beasley M. A., Hoyle F., Sharples R. M., 2002, MNRAS, 336, 168
Burstein D., Heiles C., 1982, AJ, 87, 1165
Canterna R., 1976, AJ, 81, 228
Clariá J. J., Mermilliod J.-C., Piatti A. E., Minniti D., 1994, A&AS, 107, 39
Cole A. A., 2002, Ringberg Conference on The Chemical Evolution of Dwarf Galaxies, invited talk
Cole A. A., Smecker-Hane T. A., Gallagher J. S., III, 2000, AJ, 120, 1808
Da Costa G. S., 1991, in Haynes R., Milne D., eds, The Magellanic Clouds. Kluwer, Dordrecht, 145
Da Costa G. S., Armandroff T. E., 1990, AJ, 100, 162
Friel E. F., Janes K. A., 1995, A&A, 267, 75
Gascoigne S. C. B., 1966, MNRAS, 134, 59
Geisler D., 1996, AJ, 111, 480
Geisler D., Sarajedini A., 1999, AJ, 117, 308
Geisler D., Bica E., Dottori H., Clariá J. J., Piatti A. E., Santos J. F. C., Jr, 1997, AJ, 114, 1920 (G97)
Girardi L., Bressan A., Bertelli G., Chiosi C., 2000, A&AS, 141, 371
Hesser J. E., Ugarte P. P., Hartwick F. D. A., 1976, ApJS, 32, 283
Hill V., Francois P., Spite M., Primas F., Spite F., 2000, A&A, 364, L19
Hodge P. W., 1960, ApJ, 131, 351
Hodge P. W., 1988, PASP, 100, 1051
Holtzman J. A., Gallagher J. S., III, Cole A. A., Mould J. R., Grillmair C. J., (The WFPC 2 Team), 1999, AJ, 118, 2262
Janes K. A., 1979, ApJS, 39, 135
Kontizas M., Morgan D. H., Hatzidimitriou D., Kontizas E., 1990, A&AS, 84, 527
Lauberts A., 1982, The ESO/Uppsala Survey of the ESO (B) Atlas. European Southern Observatory, Garching bei Munchen
Lejeune T., Schaerer D., 2001, A&A, 366, 538
Lejeune T., Cuisinier F., Buser R., 1997, A&AS, 125, 246
Lejeune T., Cuisinier F., Buser R., 1998, A&A, 287, 803
Leonardi A. J., Rose J. A., 2002, AJ, submitted
Lyngå G., Westerlund B., 1963, MNRAS, 127, 31
Meynet G., Mermilliod J.-C., Maeder A., 1993, A&AS, 98, 477
Mermilliod J.-C., Clariá J. J., Andersen J., Piatti A. E., Mayor M., 2001, A&A, 375, 30
Olsen K., 1999, AJ, 117, 2244
Olszewski E. W., Schommer R. A., Suntzeff N. B., Harris H. C., 1991, AJ, 101, 515
Pagel B. E. J., Tautvaišienė G., 1998, MNRAS, 299, 535
Piatti A. E., Clariá J. J., Abadi M. G., 1995, AJ, 110, 2813
Piatti A. E., Geisler D., Bica E., Clariá J. J., Santos J. F. C., Jr, Sarajedini A., Dottori H., 1999, AJ, 118, 2865
Piatti A. E., Santos J. F. C., Jr, Clariá J. J., Bica E., Sarajedini A., Geisler D., 2001, MNRAS, 325, 792
Piatti A. E., Sarajedini A., Geisler D., Bica E., Clariá J. J., 2002, MNRAS, 329, 556
Pietrzynski G., Gieren W., 2002, AJ, 124, 2633
Rich R. M., Shara M. M., Zurek D., 2001, AJ, 122, 842
Rosvick J. M., 1995, MNRAS, 277, 1379
Sarajedini A., Grocholski A. J., Levine J., Lada E., 2002, AJ, 124, 2625
Santos J. F. C., Piatti A. E., Clariá J. J., Bica E., Geisler D., Dottori H., 1999, AJ, 117, 2841
Schlegel D. J., Finkbeiner D. P., Davis M., 1998, ApJ, 500, 525
Smecker-Hane T. A., Cole A. A., Gallagher J. S., III, Stetson P. B., 2002, ApJ, 566, 239
Shapley H., Lindsay E. M., 1963, Ir. Astron. J., 6, 74
Stetson P. B., 1987, PASP, 99, 191
Westera P., Lejeune T., Buser R., 1999, in Hubery I., Heap S., Cornett R., eds, ASP Conf. Ser. Vol. 192, Spectrophotometric Dating of Stars and Galaxies. Astron. Soc. Pac., San Francisco, p. 203
Westerlund B. E., 1990, A&AR, 2, 29

This paper has been typeset from a TEX/LATEX file prepared by the author.